Journal of Materials Chemistry A

Influence of Fluorination on CO2 Adsorption in Materials Derived from Fluorinated Covalent Triazine Framework Precursors

Journal:	*Journal of Materials Chemistry A*
Manuscript ID	TA-COM-03-2019-002573.R2
Article Type:	Communication
Date Submitted by the Author:	05-Jun-2019
Complete List of Authors:	Yang, Zhenzhen; The University of Tenneessee Wang, Song; University of California, Riverside, Department of Chemistry Zhang, Zihao; The University of Tenneessee Guo, Wei; The University of Tenneessee Jie, Kecheng; The University of Tennessee, Department of Chemistry Hashim, Mohamed; University of Houston, Department of Chemistry Miljanic, Ognjen; University of Houston, Department of Chemistry Jiang, De-en; University of california at riverside Popovs, Ilja; Oak Ridge National Laboratory Dai, Sheng; Oak Ridge National Laboratory,

COMMUNICATION

Influence of Fluorination on CO_2 Adsorption in Materials Derived from Fluorinated Covalent Triazine Framework Precursors

Received 00th January 20xx,
Accepted 00th January 20xx

DOI: 10.1039/x0xx00000x

Zhenzhen Yang,[a, b] Song Wang,[c] Zihao Zhang,[a] Wei Guo,[a] Kecheng Jie,[a] Mohamed I. Hashim,[d] Ognjen Š. Miljanic,[d] De-en Jiang,[c] Ilja Popovs,[b, *] and Sheng Dai[a, b, *]

Ultra-nanoporous materials derived from fluorinated covalent triazine frameworks (CTFs) have been developed for highly efficient CO_2 capture. CO_2 uptake capacity of 6.58 mmol g^{-1} at 273 K, 1 bar (2.45 mmol g^{-1} at 0.15 bar) is achieved. The excellent performance is due to the presence of ultra-micropores (0.6~0.7 nm) that tightly fit CO_2 and strong electrostatic interactions from the residual fluorine atoms within the framework. Both molecular simulation and deep learning study predict that CTFs with F content of ~4.8 wt% and pore size distribution around ~0.7 nm can give rise to the highest CO_2 uptake capacity.

CO_2 capture and sequestration (CCS) represents a critical component of efforts aimed at reducing anthropogenic CO_2 emissions.[1-8] Aqueous alkylamine solutions are currently used for CO_2 capture in power plants but have severe energy penalties associated with regeneration of the loaded amine solution.[8-11] Physisorption based CO_2 capture using solid-state porous organic polymers (POPs) stands out as a potential alternative to liquid- or solvent-based capture techniques, due to their excellent chemical and thermal stability, tunable porosity and the ability to impart CO_2-philic functionalities for increasing the CO_2 capture performance.[1, 11-20] Nitrogen-rich covalent triazine frameworks (CTFs), a subclass of POPs, are promising candidates for CCS.[21-29] Particularly, fluorinated CTF-derived materials, e.g. FCTF-1[26] and F-DCBP-CTF,[27] are reported to exhibit enhanced CO_2 uptake capacity (5.53 and 5.98 mmol g^{-1} at 273 K, 1 bar, respectively) compared with the non-fluorinated analogues. Although several reports already discussed the potential for CO_2 capture using CTFs derived from nitrile monomers, higher CO_2 uptake capacities are still required for practical utilization in CO_2 adsorption/purification from flue gas mixtures.[23, 30] In addition, a systematic elucidation of the relationship between CO_2 capture capacity and functionality content, as well as pore size distribution, especially the presence of ultra-micropores with the dimensions close to the kinetic diameters of CO_2 (0.330 nm),[31] has not been explicitly treated, due to a paucity of available nitrile monomers. To achieve this goal, fabrication of novel CTF-derived materials with different textural structures (e.g. surface area, pore size distribution) and fluorine contents is needed and challenging, and this will rely on the rational design of aromatic nitrile monomers.

Herein, we report the synthesis of a series of tailor-made extensively fluorinated CTF derived materials, displaying high surface areas (up to 2085 m^2 g^{-1}), extensive ultra-micropores (0.5~1.6 nm) and exceptional CO_2 adsorption capacities (up to 6.58 and 4.33 mmol g^{-1} at 273 K and 298 K, respectively). The relationship between the CO_2 capacities, the residual F contents, and pore size distributions are systematically studied experimentally and by employing molecular simulations. Besides the enhancement of fluorine introduction to CO_2 uptake capacity, in this work it was found that for microporous CTF-derived materials with the same chemical composition, the optimal CO_2 uptake capacity was obtained by that with micropore size distribution around ~0.7 nm. For CTF-derived materials with the same pore size, e.g. 0.7 nm, it was found that fluorine content of ~4.8 wt% within the skeleton led to the highest CO_2 uptake capacity. This innovative approach not only enables achievement of an exceptionally high CO_2 uptake but simultaneously provides guidelines for designing POPs with an excellent performance in gas adsorption and separation.

Firstly, the fluorinated CTF derived material (**F_{12}CTF-3**) is prepared via the ionothermal technique using fluorinated tri-nitrile monomer (**F_{12}CN-3**) with heating treatment at different temperatures (Figure 1A, for details, see the Electronic Supplementary Information).[32-36] The obtained materials are denoted as **F_{12}CTF-3-T** (T is the heating temperature). For

[a] *Department of Chemistry, The University of Tennessee, Knoxville, TN, 37996, United States. E-mail: popovsi@ornl.gov; dais@ornl.gov.*
[b] *Chemical Sciences Division, Oak Ridge National Laboratory, Oak Ridge, TN 37831, United StatesChemical Sciences Division, Oak Ridge National Laboratory, Oak Ridge, TN 37831, United States.*
[c] *Department of Chemistry, University of California, Riverside, California 92521, United States.*
[d] *Department of Chemistry, University of Houston, 3585 Cullen Boulevard #112, Houston, Texas 77204-5003, United States.*
Electronic Supplementary Information (ESI) available: [details of any supplementary information available should be included here]. See DOI: 10.1039/x0xx00000x

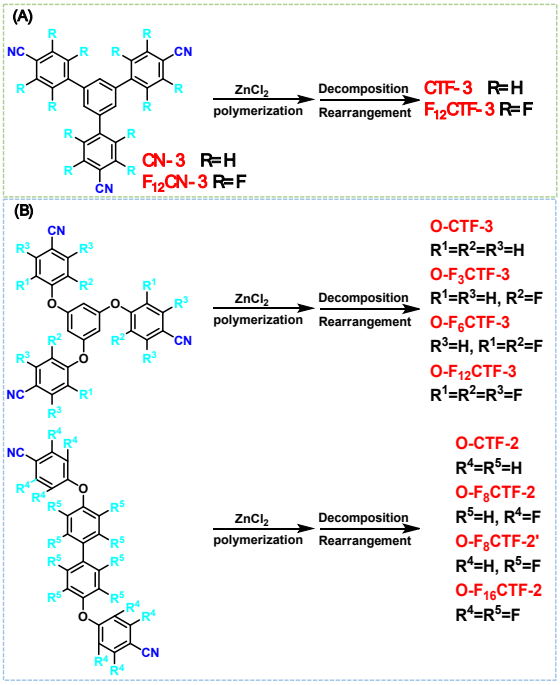

Figure 1. (A) Synthetic route and structure of CTF materials (**CTF-3** and **F_{12}CTF-3**). (B) Structures of oxygen and fluorine-bifunctionalized CTFs.

comparison, non-fluorinated **CTF-3** is also synthesized from **CN-3** with reaction temperature of 600 °C. Fourier-transform infrared spectroscopy (FT-IR) reveals the formation of triazine unit in the sample **F_{12}CTF-3-350** obtained at low temperature, with peaks located at 1327, 1388 and 1463 cm^{-1} (Figure S1).[37] C=N (1655 cm^{-1}) and its ionic intermediate form C=$N^{\delta+}$ (1709 cm^{-1}) are also present. Although the heating temperature is low, almost all the cyano groups are involved in the trimerization reaction, with no signal locating around 2251 cm^{-1}, which is obviously shown in the monomer (F_{12}CN-3). The presence of C-F bond in the monomer is evidenced by the peak displaying around 985 cm^{-1},[38] which is also observed in **F_{12}CTF-3-350**. Decomposition and rearrangement of the polymer skeleton is observed when the heating temperature increased. In the materials of **F_{12}CTF-3-450**, **F_{12}CTF-3-600**, **F_{12}CTF-3-800** and **CTF-3**, only weak peaks belonging to C=C and C-N functionalities could be observed. The solid state ^{13}C cross-polarization magic-angle-spinning (CP/MAS) NMR spectra of the the material **F_{12}CTF-3-350** shows peaks centred at 142.5 ppm and 161.1 ppm for the carbon in C-F bond and sp^2 carbons from the triazine unit, respectively.[39] The broad peak from 100~130 ppm is assigned to the signal of carbons in the benzene ring. While for materials obtained by further increasing the heating temperature to 450~800 °C, only one broad peak ranging from 100~170 ppm is present, indicating decomposition and rearrangement of the material structures. X-ray power diffraction (XRD) patterns for **F_{12}CTF-3-T** and **CTF-3** show that the whole structures of the materials obtained in this work are amorphous (Figure S3).

F_{12}CTF-3-600 (referred as **F_{12}CTF-3**) is selected for further characterization. Raman spectrum of **F_{12}CTF-3** shows both peaks for structure defects (ID) and graphitic carbon (IG), with the intensity ratio of 1.07 (Figure S4). The chemical state and electronic state of the elements in **F_{12}CTF-3** are investigated by X-ray photoelectron spectroscopy (XPS) (Figure S5). The obtained C1s spectrum supports the existence of aromatic C (284.08 eV), C-N bond (285.38 eV) and residual amount of C-F bond (288.68 eV). N1s spectrum indicates the presence of pyridinic (397.87 eV, 26.0%) and pyrrolic nitrogen (400.33 eV, 74.0%). Despite the high temperature used during the synthesis of **F_{12}CTF-3** (up to 600 °C), the residual fluorine content of up to 3.7 wt% is still present in the material, with the two peaks in its F1s spectrum that correspond to semi-ionic (687.8 eV) and covalent C-F bonds (689.2 eV).

Nitrogen sorption studies at 77 K (Figure 2A) show a first step at P/P_0<0.05, corresponding to gas sorption in micropores. **F_{12}CTF-3** exhibits a typical type I isotherm, implying a solely microporous structure. For **CTF-3**, the sorption isotherm (Type IV) of the material shows a further uptake of N_2 in the medium relative pressure region as well as a small hysteresis, reflecting a substantial contribution of additional small mesopores. The Brunauer-Emmett-Teller (BET) surface areas are evaluated to be 1558 and 1454 m^2 g^{-1} for **F_{12}CTF-3** and **CTF-3**, respectively (Figure S6). The pore-size of **F_{12}CTF-3** calculated by non-linear density functional theory (NLDFT) shows well-defined ultra-nanopore distributions at 0.6~0.7 nm (Figure 2B). In contrast, **CTF-3** has major peaks centred at 1.0 nm and 3.0 nm with a significantly broader distribution. Replacing H atoms with F atoms in the starting material apparently results in the CTFs with a reduced effective pore size. In addition, the total pore volume in **F_{12}CTF-3** (1.32 cm^3 g^{-1}) is higher than that in **CTF-3** (0.98 cm^3 g^{-1}).

The CO_2 adsorption performance of **F_{12}CTF-3** is assessed by CO_2 isotherms at 273 K and 298 K (Figure 2C). Notably, although BET surface area of **F_{12}CTF-3** is only marginally higher than that of **CTF-3**, **F_{12}CTF-3** exhibits a significantly higher CO_2 adsorption capacity at 1 bar (6.58 mmol g^{-1} at 273 K and 4.33 mmol g^{-1} at 298 K), almost two times higher than that of **CTF-3** (2.13 mmol g^{-1} at 273 K and 1.34 mmol g^{-1} at 298 K). Adsorption of CO_2 at ~0.15 bar is more relevant to practical CO_2 capture since flue gas contains ~15% CO_2 at total pressure of ~1 bar.[1] It can be seen that at low CO_2 pressure (0.15 bar) and 273 K, **F_{12}CTF-3** adsorbs 2.45 mmol g^{-1} CO_2, remaining significantly higher than **CTF-3** (0.57 mmol g^{-1}). Notably, at 273 K, **F_{12}CTF-3** exhibits a higher CO_2 uptake capacity at 0.15 bar (2.45 mmol g^{-1}) compared to **CTF-3** at 1 bar (2.13 mmol g^{-1}). The CO_2 uptake of **F_{12}CTF-3** at 273 K and 1 bar is among the highest CO_2 capacities for all POP-based adsorbents reported so far (Table S1). For example, a porous polymer framework (**PPF-1**) via imine condensation shows a CO_2 capacity of 6.07 mmol g^{-1} (273 K, 1 bar).[40] Among various CTF materials, **bipyridine-CTF** synthesized at 600 °C exhibited a CO_2 uptake capacity of 5.58 mmol g^{-1} (273 K, 1 bar).[22] The best CTF-based adsorbent up to now was obtained by our group via an *in situ* doping strategy. The generated hexaazatriphenylene-based CTF (**HAT-CTF-450/600**) exhibited high CO_2 uptake capacities (6.3 mmol g^{-1} at 273, 1 bar).[21] The performance of **F_{12}CTF-3** in this study even surpasses the CO_2 uptake capacity of the N-doped hierarchical

carbon decorated with ultra-small pores (d < 0.5 nm) (**SU-MAC-500**), showing an impressive CO_2 uptake of

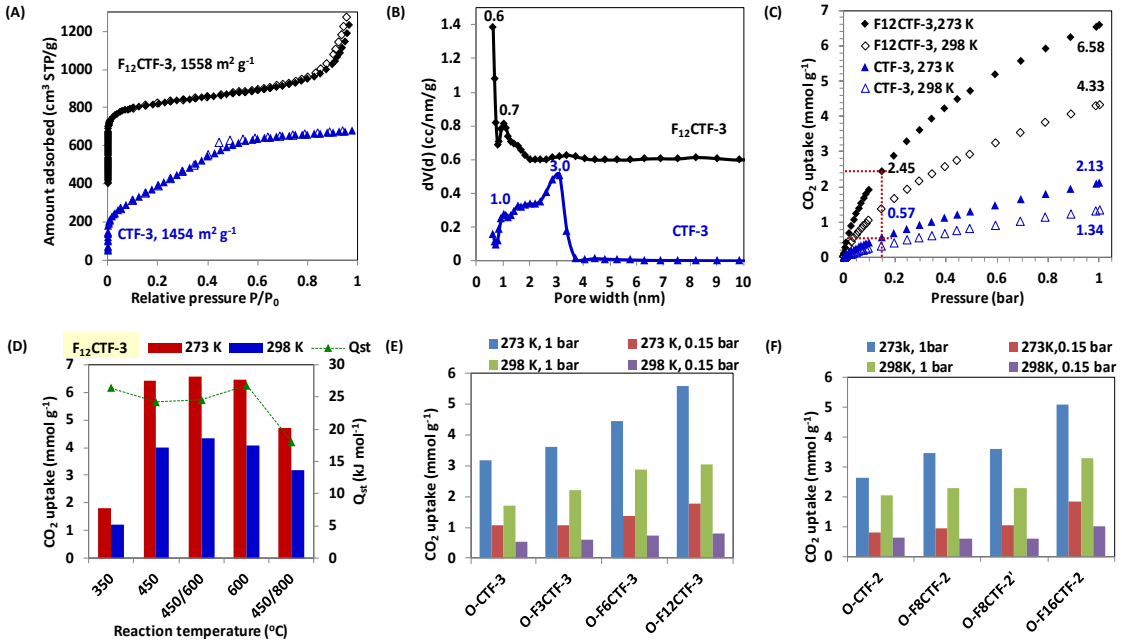

Figure 2. (A) Nitrogen isotherms, (B) pore size distributions, (C) CO_2 uptake isotherms and (D) CO_2 adsorption capacities at 1 bar and Q_{st} for **F_{12}CTF-3** synthesized at different temperatures. (E) CO_2 uptake capacities at 0.15 and 1 bar for oxygen and fluorine bifunctionalized **O-CTF-3** and (F) **O-CTF-2**.

6.03 mmol g^{-1} (273 K, 1 bar).[41] Very recently, a covalent quinazoline networks (CQNs) was reported showing CO_2 capacity of 7.16 mmol g^{-1} at 273 K and 1 bar.[18] Notably, **F_{12}CTF-3** also exhibits much higher CO_2 selectivity over N_2 and CH_4 compared to **CTF-3** (Figure S7). The isosteric heats of adsorption (Q_{st}) at low adsorption values are calculated to be 24.5 and 21.0 kJ mol^{-1} for **F_{12}CTF-3** and **CTF-3**, respectively, indicating a stronger dipole-quadrupole interaction between the polarizable CO_2 molecules and the **F_{12}CTF-3** framework (Figure S8).

It is well-known that ionothermal reaction temperature has a profound effect on the structural properties of the resultant CTFs.[21, 32, 34, 42] CO_2 Adsorption capacity of the resultant **F_{12}CTF-3-T** (T represents the temperature) is investigated. As shown in Figure 2D and Table S2, although the BET surface areas increase in order: **F_{12}CTF-3-350** < **F_{12}CTF-3-450** < **F_{12}CTF-3-600** < **F_{12}CTF-3-450/600** < **F_{12}CTF-3-800**, materials obtained at 450~600 °C exhibit similar CO_2 uptake capacities, in the range of 6.43~6.58 mmol g^{-1} at 273 K and 1 bar. Comparatively, **HAT-CTF-450** reported by our group only had CO_2 capacity of 4.4 mmol g^{-1} at 273 K and 1 bar.[21] This is probably due to the high reactivity of the fluorinated monomers, which ensure that the trimerization of the nitrile groups is almost complete at 450 °C. In contrast, **F_{12}CTF-3-350** only shows a low CO_2 capacity of 1.79 mmol g^{-1}, probably owing to its low surface are (842 m^2 g^{-1}) compared with materials obtained at higher temperature (450~800 °C). Thermogravimetric analysis (TGA) of **F_{12}CTF-3-350** indicates that it begins to decompose at ~450 °C (Figure S9). As the reaction temperature increases to 800 °C, although the resultant **F_{12}CTF-3-800** has the highest BET surface area (2085 m^2 g^{-1}), its CO_2 capacity is only 4.70 mmol g^{-1} at 273 K and 1 bar. XPS analysis of **F_{12}CTF-3-T** shows that the residual fluorine content in the materials decreases as the ionothermal temperature increases, from 16.06 wt% in **F_{12}CTF-3-350** to 2.74 wt% in **F_{12}CTF-3-800** (Table S2). The weakening in the CO_2-sorbent interactions is evident from the decreased Q_{st}, 24.2~26.8 kJ mol^{-1} for CTFs obtained at 350~600 °C (Figure S10), while only 18 kJ mol^{-1} for **F_{12}CTF-3-800**, indicating the important role of CO_2-philic F atoms present within the framework.[43-45] From the structure characterization viewpoint, it appears that neither the specific surface area nor the total pore volume directly contribute to the CO_2 capacities (Table S2 and Figure S11). Compared with the results obtained for **F_{12}CTF-3-600**, **F_{12}CTF-3-450** shows higher surface area, CO_2-philic N and F contents, while it exhibits similar CO_2 uptake capacity with **F_{12}CTF-3-600**. This was probably due to the higher composition of ultra-micropores (~0.5 nm) in **F_{12}CTF-3-600** (Figure S11). With the increase of the reaction temperature, pore size distributions in the obtained CTFs show that the 0.5 and 1.1 nm peaks decrease in intensity, while the 1.6 and 2.5 nm peaks increase. This suggests that high-temperature leads to further loss of fluorine and creates additional volume of wider pores within the CTF frameworks. Therefore, high adsorption capacity of fluorinated CTF derived material towards CO_2 is due to presence of ultramicropores (<1.1 nm) that tightly fit CO_2 and strong electrostatics from F atoms that line the pore surface.

To further uncover the impact of fluorination on the CO_2 capacities, two other kinds of ether group-linked di- and trinitriles (**O-F_nCN-3/2**) with different number of fluorine

substituents on the benzene rings are designed and the corresponding CTF derived materials are obtained through ionothermal method (Figure 1B and Scheme S1, for details, see the Electronic Supplementary Information). As shown in Figure 2E and 2F, from **O-CTF-3** to **O-F$_{12}$CTF-3**, and **O-CTF-2** to **O-F$_{16}$CTF-2**, the CO_2 adsorption capacities at 273 K and 298 K increase as the number of F atoms on the benzene rings increases (Table S3). Notably, the position of the F-substituted benzene rings only has small effect on the final CO_2 uptake performance, as similar CO_2 capacities for **O-F$_8$CTF-2** and **O-F$_8$CTF-2'** are obtained. To gain further insight into the influences of various parameters on CO_2 uptake, elemental (C, H, N and F) analysis of **O-CTF-2** with different fluorine content is conducted (Table S4). Notably, the fluorine content in **O-F$_8$CTF-2** and **O-F$_8$CTF-2'** is 0.78 wt% and 4.46 wt%, respectively, despite the same fluorine content in their precursor (28.6 wt%), probably owing to the loss of fluorinated benzene ring through ether group cleavage. The nitrogen content in **O-F$_8$CTF-2** (4.08 wt%) and **O-F$_8$CTF-2'** (4.24 wt%) shows no significant difference. Correspondingly, elimination of more fluorine atoms is estimated to give material with higher surface area. Indeed, **O-F$_8$CTF-2** shows higher BET surface area (1878 m^2 g^{-1}) than that of **O-F$_8$CTF-2'** (1403 m^2 g^{-1}). As shown in Figure 2F, **O-F$_8$CTF-2** and **O-F$_8$CTF-2'** exhibit similar CO_2 uptake capacities, which is in opposite trend with the surface area. Therefore, we can conclude that high fluorine content plays important role in the CO_2 uptake enhancement.

Molecular simulations of CO_2 adsorption were performed to further understand the CO_2 sorption behavior. However, as shown by the structural characterization results, the whole structures of the CTF-derived materials are amorphous, which is difficult to be investigated using molecular simulation. In addition, several parameters are involved and influence the CO_2 uptake capacities of the materials. We need to figure out a way to make variation of only one parameter while keep others under the same conditions. Therefore, in the following work, crystalline skeletons are adopted, trying to gain some tendency about the influence of pore size distributions and fluorine contents on the CO_2 uptake capacities. Dispersion-corrected density functional theory calculations (DTF-D3) were performed with the Vienna ab initio simulation package (VASP) to optimize the cells and structures of **CTF-3** and **F$_{12}$CTF-3**. The Perdew–Burke–Ernzerhof (PBE) form of the generalized-gradient approximation (GGA) was used for electron exchange and correlation. The projector-augmented-wave (PAW) method was used to describe the electron-core interaction with the cutoff energy of 450 eV for the planewave bases. To simulate the uptake of CO_2, grand canonical Monte Carlo (GCMC) simulations (constant chemical potential μ, volume V and temperature T) were carried out for the porous materials with a slit-pore model based on the experimental pore size distributions. The CO_2 adsorption data were fitted using the virial equation. The pore sizes of 0.6 nm, 0.7 nm and 1.0 nm, 3.0 nm were used for **F$_{12}$CTF-3** and **CTF-3**, respectively. The universal force field (UFF) parameters were chosen for CTFs and CO_2. The partial atomic charges of CTFs were calculated by the Repeating Electrostatic Potential Extracted Atomic charges (REPEAT) method based on DFT-derived electrostatic potential. All GCMC simulations were run for 107 steps to obtain sufficient statistics.

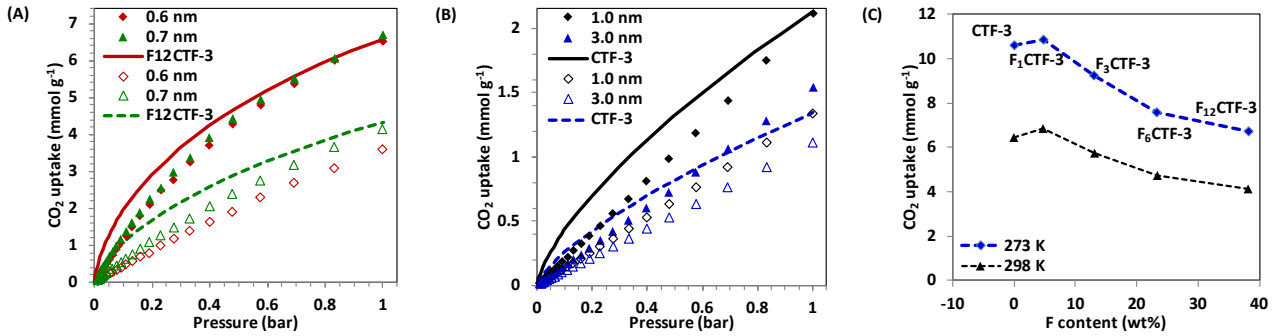

Figure 3. The simulated (symbol) and measured CO2 adsorption data (line) of (A) **F$_{12}$CTF-3** and (B) **CTF-3** at 273 K (solid line and symbol) and 298 K (dashed line and hollow symbol). (C) Simulated CO_2 uptake by **CTF-3** having pore size of 0.7 nm with different F content.

For **F$_{12}$CTF-3**, at 273 K, pores with diameters of 0.6 and 0.7 nm shows similar simulated CO_2 uptake, which fits well with the experimental result (Figure 3A). At 298 K, material with pore size of 0.7 nm shows higher simulated CO_2 sorption performance than that with 0.6 nm, which is closer to the experimental result. This is also in accordance with the previous reports that a cylindrical pore size between 0.7 and 0.8 nm would be most beneficial for CO_2 capture with the maximum potential energy surface (PES) overlap and maximum amount of CO_2 adsorbed.[46] For **CTF-3**, the simulated CO_2 uptake with material having pore size of 1.0 nm is closer to the experimental results both at 273 K and 298 K, which is obviously higher than that with pore size of 3.0 nm (Figure 3B). The snapshots of CO_2 distribution at 1 bar show that CO_2 molecules mainly locate within the interlayer space of the CTF materials (Figure S12). To study the influence of F content, **CTF-3** materials with different number of fluorine atoms on the backbone are employed, and the simulation results showed that the highest CO_2 uptake capacity (10.88 mmol g^{-1} at 273 K) is obtained by **F$_1$CTF-3**, corresponding to F content of 4.8 wt% (Figure 3C, Table S5 and Figure S13). Higher F content leads to decreased CO_2 uptake capacity, mainly due to the higher molecular weight of F compared with H. Enhanced CO_2 uptake by F introduction is also evidenced by the predicted CO_2 uptake using a deep learning method (Table S6).[47] The result shows that, with the same surface areas, total pore volumes and micropore volumes, CTFs

with F content of < 7 wt% obtained in this work exhibit much higher CO_2 capacity compared with carbon materials. However, if the F content in **F_{12}CTF-3-350** is too high, e.g. 16 wt%, lower CO_2 capacity will be obtained compared with carbons under otherwise identical conditions.

Conclusions

In conclusion, a novel fluorinated ultra nanoporous CTF material (**F_{12}CTF-3**) has been developed, exhibiting CO_2 uptake capacity of 6.58 mmol g^{-1} at 273 K and 1 bar, which is among the highest values of the known POPs. High CO_2 uptake (6.43 mmol g^{-1} at 273 K, 1 bar) can be maintained with material synthesized at low temperature (450 °C). Molecular simulations and deep learning study provide further rationale of the importance of optimal fluorine content in the residual structure in combination with narrow nanopore distribution on the observed CO_2 capacity and selectivity. Our study underscores the role of fluorine not only as a CO_2-philic group but also as porosity forming group, in turn providing guidelines towards the rational design and development of new nanoporous materials for efficient CO_2 capture.

Conflicts of interest

There are no conflicts to declare.

Acknowledgements

The research was supported financially by the Division of Chemical Sciences, Geosciences, and Biosciences, Office of Basic Energy Sciences and US Department of Energy. O. Š. M. and M. I. H. acknowledge generous financial support from the the Welch Foundation (grant E-1768) and the National Science Foundation (grant DMR-1507664).

Notes and references

1. M. Oschatz and M. Antonietti, *Energy Environ. Sci.*, 2018, **11**, 57-70.
2. R. Monastersky, *Nature*, 2013, **497**, 13.
3. M. E. Boot-Handford, J. C. Abanades, E. J. Anthony, M. J. Blunt, S. Brandani, N. Mac Dowell, J. R. Fernandez, M.-C. Ferrari, R. Gross, J. P. Hallett, R. S. Haszeldine, P. Heptonstall, A. Lyngfelt, Z. Makuch, E. Mangano, R. T. J. Porter, M. Pourkashanian, G. T. Rochelle, N. Shah, J. G. Yao and P. S. Fennell, *Energy Environ. Sci.*, 2014, **7**, 130-189.
4. J. M. Huck, L.-C. Lin, A. H. Berger, M. N. Shahrak, R. L. Martin, A. S. Bhown, M. Haranczyk, K. Reuter and B. Smit, *Energy Environ. Sci.*, 2014, **7**, 4132-4146.
5. J. Wang, L. Huang, R. Yang, Z. Zhang, J. Wu, Y. Gao, Q. Wang, D. O'Hare and Z. Zhong, *Energy Environ. Sci.*, 2014, **7**, 3478-3518.
6. Z. Zhang, Z.-Z. Yao, S. Xiang and B. Chen, *Energy Environ. Sci.*, 2014, **7**, 2868-2899.
7. S. J. Datta, C. Khumnoon, Z. H. Lee, W. K. Moon, S. Docao, T. H. Nguyen, I. C. Hwang, D. Moon, P. Oleynikov, O. Terasaki and K. B. Yoon, *Science*, 2015, **350**, 302-306.
8. K. Min, W. Choi, C. Kim and M. Choi, *Nat. Commun.*, 2018, **9**, 726.
9. G. T. Rochelle, *Science*, 2009, **325**, 1652-1654.
10. D. M. D'Alessandro, B. Smit and J. R. Long, *Angew. Chem. Int. Ed.*, 2010, **49**, 6058-6082.
11. H. A. Patel, J. Byun and C. T. Yavuz, *ChemSusChem*, 2016, **10**, 1303-1317.
12. L. Zou, Y. Sun, S. Che, X. Yang, X. Wang, M. Bosch, Q. Wang, H. Li, M. Smith, S. Yuan, Z. Perry and H.-C. Zhou, *Adv. Mater.*, 2017, **29**, 1700229.
13. X. Zou and G. Zhu, *Adv. Mater.*, 2017, **30**, 1700750.
14. X.-Y. Yang, L.-H. Chen, Y. Li, J. C. Rooke, C. Sanchez and B.-L. Su, *Chem. Soc. Rev.*, 2017, **46**, 481-558.
15. W. Wang, M. Zhou and D. Yuan, *J. Mater. Chem. A*, 2017, **5**, 1334-1347.
16. L. Tan and B. Tan, *Chem. Soc. Rev.*, 2017, **46**, 3322-3356.
17. S. Das, P. Heasman, T. Ben and S. Qiu, *Chem. Rev.*, 2017, **117**, 1515-1563.
18. O. Buyukcakir, R. Yuksel, Y. Jiang, S. H. Lee, W. K. Seong, X. Chen and R. S. Ruoff, *Angew. Chem. Int. Ed.*, 2018, DOI: 10.1002/anie.201813075, DOI: 10.1002/anie.201813075.
19. P. Li, Y. He, Y. Zhao, L. Weng, H. Wang, R. Krishna, H. Wu, W. Zhou, M. O'Keeffe, Y. Han and B. Chen, *Angew. Chem. Int. Ed.*, 2015, **54**, 574-577.
20. Q. Sun, Y. Jin, B. Aguila, X. Meng, S. Ma and F.-S. Xiao, *ChemSusChem*, 2016, **10**, 1160-1165.
21. X. Zhu, C. Tian, G. M. Veith, C. W. Abney, J. Dehaudt and S. Dai, *J. Am. Chem. Soc.*, 2016, **138**, 11497-11500.
22. S. Hug, L. Stegbauer, H. Oh, M. Hirscher and B. V. Lotsch, *Chem. Mater.*, 2015, **27**, 8001-8010.
23. A. Bhunia, V. Vasylyeva and C. Janiak, *Chem. Commun.*, 2013, **49**, 3961-3963.
24. P. Katekomol, J. Roeser, M. Bojdys, J. Weber and A. Thomas, *Chem. Mater.*, 2013, **25**, 1542-1548.
25. S. Hug, M. B. Mesch, H. Oh, N. Popp, M. Hirscher, J. Senker and B. V. Lotsch, *J. Mater. Chem. A*, 2014, **2**, 5928-5936.
26. Y. Zhao, K. X. Yao, B. Teng, T. Zhang and Y. Han, *Energy Environ. Sci.*, 2013, **6**, 3684-3692.
27. G. Wang, K. Leus, H. S. Jena, C. Krishnaraj, S. Zhao, H. Depauw, N. Tahir, Y.-Y. Liu and P. Van Der Voort, *J. Mater. Chem. A*, 2018, **6**, 6370-6375.
28. K. Wang, L.-M. Yang, X. Wang, L. Guo, G. Cheng, C. Zhang, S. Jin, B. Tan and A. Cooper, *Angew. Chem. Int. Ed.*, 2017, **56**, 14149-14153.
29. X. Zhu, C. Tian, S. M. Mahurin, S.-H. Chai, C. Wang, S. Brown, G. M. Veith, H. Luo, H. Liu and S. Dai, *J. Am. Chem. Soc.*, 2012, **134**, 10478-10484.
30. R. Walczak, B. Kurpil, A. Savateev, T. Heil, J. Schmidt, Q. Qin, M. Antonietti and M. Oschatz, *Angew. Chem. Int. Ed.*, 2018, **57**, 10765-10770.
31. M. Zaworotko, K.-J. Chen, Q.-Y. Yang, S. Sen, D. Madden, A. Kumar, T. Pham, K. Forrest, N. Hosono, B. Space and S. Kitagwa, *Angew. Chem. Int. Ed.*, 2018, **57**, 3332-3336.
32. P. Kuhn, M. Antonietti and A. Thomas, *Angew. Chem. Int. Ed.*, 2008, **47**, 3450-3453.
33. M. J. Bojdys, J. Jeromenok, A. Thomas and M. Antonietti, *Adv. Mater.*, 2010, **22**, 2202-2205.
34. P. Puthiaraj, Y.-R. Lee, S. Zhang and W.-S. Ahn, *J. Mater. Chem. A*, 2016, **4**, 16288-16311.
35. T.-H. Chen, I. Popov, W. Kaveevivitchai, Y.-C. Chuang, Y.-S. Chen, A. J. Jacobson and O. Š. Miljanić, *Angew. Chem. Int. Ed.*, 2015, **54**, 13902-13906.
36. M. I. Hashim, H. T. M. Le, T.-H. Chen, Y.-S. Chen, O. Daugulis, C.-W. Hsu, A. J. Jacobson, W. Kaveevivitchai, X. Liang, T. Makarenko,

O. Š. Miljanić, I. Popovs, H. V. Tran, X. Wang, C.-H. Wu and J. I. Wu, *J. Am. Chem. Soc.*, 2018, **140**, 6014-6026.
37. J. Liu, P. Lyu, Y. Zhang, P. Nachtigall and Y. Xu, *Adv. Mater.*, 2018, **30**, 1705401.
38. M. Álvarez-Paino, A. Muñoz-Bonilla, G. Marcelo, J. Rodríguez-Hernández and M. Fernández-García, *Polym. Chem.*, 2012, **3**, 3282-3288.
39. M. Liu, K. Jiang, X. Ding, S. Wang, C. Zhang, J. Liu, Z. Zhan, G. Cheng, B. Li, H. Chen, S. Jin and B. Tan, *Adv. Mater.*, 2019, DOI: 10.1002/adma.201807865, e1807865.
40. Y. Zhu, H. Long and W. Zhang, *Chem. Mater.*, 2013, **25**, 1630-1635.
41. J. W. F. To, J. He, J. Mei, R. Haghpanah, Z. Chen, T. Kurosawa, S. Chen, W.-G. Bae, L. Pan, J. B. H. Tok, J. Wilcox and Z. Bao, *J. Am. Chem. Soc.*, 2016, **138**, 1001-1009.
42. P. Kuhn, A. Thomas and M. Antonietti, *Macromolecules*, 2009, **42**, 319-326.
43. J. B. McClain, D. E. Betts, D. A. Canelas, E. T. Samulski, J. M. DeSimone, J. D. Londono, H. D. Cochran, G. D. Wignall, D. Chillura-Martino and R. Triolo, *Science*, 1996, **274**, 2049-2052.
44. J. M. DeSimone, E. E. Maury, Y. Z. Menceloglu, J. B. McClain, T. J. Romack and J. R. Combes, *Science*, 1994, **265**, 356-359.
45. J. M. DeSimone, Z. Guan and C. S. Elsbernd, *Science*, 1992, **257**, 945-947.
46. S. Wang, Z. Tian, S. Dai and D.-e. Jiang, *J. Phys. Chem. C*, 2017, **121**, 22025-22030.
47. Z. Zhang, J. A. Schott, M. Liu, H. Chen, X. Lu, B. G. Sumpter, J. Fu and S. Dai, *Angew. Chem. Int. Ed.*, 2019, **58**, 259-263.

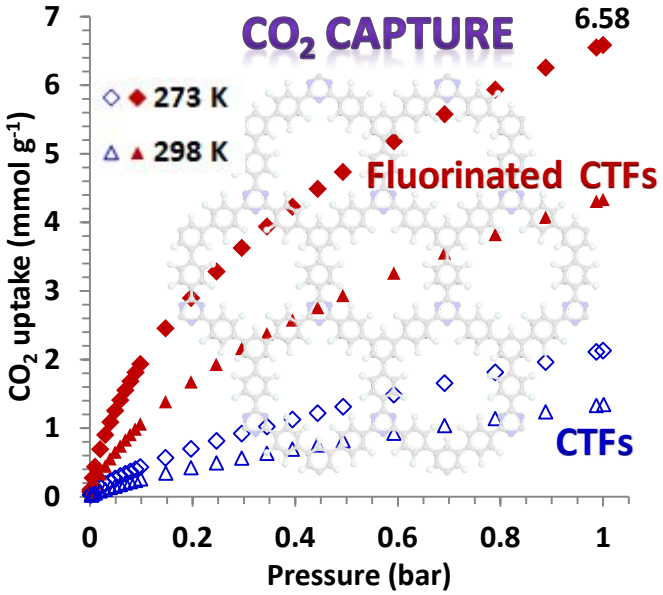

Give me more fluorines: Controlled introduction of fluorine in the structure of Covalent Triazine Frameworks (CTFs) can improve their CO_2 adsorption. Materials with optimal fluorine content in the residual structure in combination with narrow nanopore distribution are promising CO_2 scavengers.